

Article

Calculation of the Acoustic Spectrum of a Cylindrical Vortex in Viscous Heat-Conducting Gas Based on the Navier–Stokes Equations

Tatiana Petrova * and Fedor Shugaev

Department of Quantum Statistics and Field Theory, Faculty of Physics,

M.V. Lomonosov Moscow State University, Leninskie Gory, 1-2, 119991 Moscow, Russia; shugaev@physics.msu.ru

* Correspondence: tapetrova@physics.msu.ru; Tel.: +7-495-939-1215

Academic Editor: Ali Cemal Benim

Received: 6 July 2016; Accepted: 15 August 2016; Published: 20 August 2016

Abstract: An extremely interesting problem in aero-hydrodynamics is the sound radiation of a single vortical structure. Currently, this type of problem is mainly considered for an incompressible medium. In this paper a method was developed to take into account the viscosity and thermal conductivity of gas. The acoustic radiation frequency of a cylindrical vortex on a flat wall in viscous heat-conducting gas (air) has been investigated. The problem is solved on the basis of the Navier–Stokes equations using the small initial vorticity approach. The power expansion of unknown functions in a series with a small parameter (vorticity) is used. It is shown that there are high-frequency oscillations modulated by a low-frequency signal. The value of the high frequency remains constant for a long period of time. Thus the high frequency can be considered a natural frequency of the vortex radiation. The value of the natural frequency depends only on the initial radius of the cylindrical vortex, and does not depend on the intensity of the initial vorticity. As expected from physical considerations, the natural frequency decreases exponentially as the initial radius of the cylinder increases. Furthermore, the natural frequency differs from that of the oscillations inside the initial cylinder and in the outer domain. The results of the paper may be of interest for aeroacoustics and tornado modeling.

Keywords: Navier–Stokes equations; cylindrical vortex; acoustic radiation; heat-conducting gas

1. Introduction

Vortical structures (vortex rings and cylindrical vortices) play an important role in the sound radiation of gaseous flows. The general problems of sound radiation of vortices are considered in [1,2]. Research on the radiation of vortex systems has been conducted in [3] (system of two vortex rings) and [4] (system of four cylindrical vortices). The computations were performed with the aid of a vortex particle method [5]. Analysis of perturbation energy of eddy flows in connection with the problem of stability was considered in [6–9].

It should also be mentioned that in the LES (Large Eddy Simulation), turbulence is simulated as a set of large-scale vortices [10]. In this regard, the study of individual vortex dynamics and of its acoustic radiation is of interest.

Sound generation by a single cylindrical vortex is of special interest. Unfortunately, this problem was analyzed only for non-viscous fluid [11,12].

However, the presence of viscosity is responsible for the occurrence of tangential stresses, and they generate vorticity. Thus, vortical structures can be regarded as substantially non-linear objects and described based on the Navier–Stokes equations, taking into account the viscosity and thermal conductivity of the medium.

We set forth a method for the calculation of multiple integrals which reduces the solution to partial differential equations. This method is very promising for aeroacoustic problems, since it allows

analysis of the sound generation of a single cylindrical vortex. Until now, researchers have analyzed the sound generation during the interaction of vortices and vortex-acoustic interaction.

The method can be useful to simulate a tornado, and the results of its application to the cylindrical vortex are of interest for aeroacoustics and description of characteristics of turbulent flow. The aim of this paper is to investigate the acoustic radiation of a cylindrical vortex on a flat wall.

2. Governing Equations

The Navier–Stokes equations are derived by applying Newton’s Law of Motion to a fluid element. It is supplemented by the mass continuity equation and the energy equation. The system also includes the momentum equation. They are valid if the characteristic length is much greater than the free path distance of molecules. The Navier–Stokes equations take into account vorticity diffusion and energy dissipation in contrast to the Euler equations.

The non-stationary system of the Navier–Stokes equations is:

$$\begin{cases} \rho \frac{dv_i}{dt} = \frac{\partial P_{ij}}{\partial x_j}, \\ \frac{d\rho}{dt} + \rho \frac{\partial v_k}{\partial x_k} = 0, \\ \rho \frac{de}{dt} = P_{ij} \dot{\epsilon}_{ij} + \frac{\partial}{\partial x_j} (\lambda \frac{\partial T}{\partial x_j}). \end{cases} \quad (1)$$

$$\frac{d}{dt} = \frac{\partial}{\partial t} + v_j \frac{\partial}{\partial x_j}, P_{ij} = 2\mu \dot{\epsilon}_{ij} - \frac{2}{3} \mu \dot{\epsilon}_{kk} \delta_{ij} - p \delta_{ij}, \dot{\epsilon}_{ij} = \frac{1}{2} (\frac{\partial v_i}{\partial x_j} + \frac{\partial v_j}{\partial x_i}), e = C_V T.$$

We use the Helmholtz decomposition of the velocity field into a potential part and a solenoidal one

$$\vec{v}(\vec{x}, t) = -\frac{\vec{\nabla}}{4\pi} \int \frac{s(\vec{\xi}, t)}{|\vec{x} - \vec{\xi}|} d\vec{\xi} + \frac{1}{4\pi} \vec{\nabla} \times \int \frac{\vec{\Omega}(\vec{\xi}, t)}{|\vec{x} - \vec{\xi}|} d\vec{\xi}; \quad (2)$$

$$s = \vec{\nabla} \cdot \vec{v}, \vec{\Omega} = \vec{\nabla} \times \vec{v}, \vec{\nabla} = (\frac{\partial}{\partial x_1}; \frac{\partial}{\partial x_2}; \frac{\partial}{\partial x_3}).$$

Taking into account Equation (2), the Navier–Stokes System (1) in dimensionless form can be written as follows:

$$\begin{cases} \frac{\partial \Omega_i}{\partial t} = \nu \Delta \Omega_i + \frac{3}{4} \dot{\epsilon}_{ijk} \nu (\frac{\partial v_k}{\partial x_m} + \frac{\partial v_m}{\partial x_k}) \frac{\partial^2 h}{\partial x_j \partial x_m} - v_j \frac{\partial \Omega_i}{\partial x_j} + \Omega_m \frac{\partial v_i}{\partial x_m} - s \Omega_i + f_{1i}, \\ \frac{\partial w}{\partial t} = -v_j \frac{\partial w}{\partial x_j} + s, \\ \frac{\partial s}{\partial t} = \frac{e^h}{\gamma} \Delta w + \frac{4}{3} \nu \Delta s - (\frac{1}{\gamma} e^h + 0.5sv) \Delta h + 1.5 \nu \frac{\partial v_i}{\partial x_j} \frac{\partial^2 h}{\partial x_i \partial x_j} - v_j \frac{\partial s}{\partial x_j} + f_2, \\ \frac{\partial h}{\partial t} = \frac{\gamma}{Pr} \eta \Delta h - (\gamma - 1)s - v_j \frac{\partial h}{\partial x_j} + f_3, \end{cases} \quad (3)$$

$$w = -\text{Log} \rho, h = \text{Log} T, \nu = \mu / \rho, \eta = \lambda / \rho, \\ \Delta = \frac{\partial^2}{\partial x_i \partial x_i}, i = 1, 2, 3, j = 1, 2, 3, k = 1, 2, 3, m = 1, 2, 3.$$

Here ϵ_{ijl} is the antisymmetrical tensor, Δ is Laplacian, ρ, T, \vec{v} are dimensionless values of density, temperature, velocity (divided by ρ_0, T_0, c_0 , respectively), μ, ν, λ, c is viscosity, kinematic viscosity, heat conductivity and low-frequency sound speed, γ is the adiabatic exponent, and Pr is the Prandtl number.

The functions f_{1i}, f_2, f_3 are non-linear terms with respect to the first derivatives over coordinates. Subscript “0” refers to the initial state which is supposed to be uniform.

The System (3) was made dimensionless using the characteristic length $l_0 = \nu_0 / c_0$ and the characteristic time $t_0 = \nu_0 / c_0^2$. The dependence of air viscosity and thermal conductivity on temperature can be described as a power law: $\mu / \mu_0 = T^{0.75}, \lambda / \lambda_0 = T^{0.75}$.

Pressure, temperature and density are related to the Mendeleev–Clapeyron equation $p = \frac{\rho RT}{M}$, M being molar mass.

2.1. The Initial Value Problem

At the initial instant the vorticity has a non-zero value ω_0 only within a gaseous circular cylinder of a radius r_0 and of a height z_0 . The cylinder is situated on a flat wall. The axis of the cylinder is normal to the wall (4).

The problem is considered under the assumption that the initial vorticity ω_0 is small ($\omega_0 \ll 1$). The initial conditions are:

$$\begin{aligned} \Omega_z(\vec{x}, 0) &= \begin{cases} \omega_0, r \leq r_0 \\ 0, r > r_0 \end{cases} \\ w(\vec{x}, 0) = s(\vec{x}, 0) = h(\vec{x}, 0) &= 0. \end{aligned} \tag{4}$$

The velocity on the flat wall is equal to zero: $\vec{v}(\vec{x}, t)|_{z=0} = 0$. The solution does not depend on φ (r, φ, z being cylindrical coordinates).

2.2. The Solution to the Problem

In order to solve Equation (3) let us expand the unknown functions in power series of a small parameter $\varepsilon = \omega_0$. We get:

$$\begin{aligned} \Omega_1^{(1)}(\vec{x}, t) &= \varepsilon^2 \Omega_1^{(1)}(\vec{x}, t) + \varepsilon^3 \Omega_1^{(2)}(\vec{x}, t) + \varepsilon^4 \Omega_1^{(3)}(\vec{x}, t) + \dots, \\ \Omega_2^{(1)}(\vec{x}, t) &= \varepsilon^2 \Omega_2^{(1)}(\vec{x}, t) + \varepsilon^3 \Omega_2^{(2)}(\vec{x}, t) + \varepsilon^4 \Omega_2^{(3)}(\vec{x}, t) + \dots, \\ \Omega_3(\vec{x}, t) &= \varepsilon \Omega_3^{(1)}(\vec{x}, t) + \varepsilon^2 \Omega_3^{(2)}(\vec{x}, t) + \varepsilon^3 \Omega_3^{(3)}(\vec{x}, t) + \dots, \\ w(\vec{x}, t) &= \varepsilon^2 w^{(1)}(\vec{x}, t) + \varepsilon^3 w^{(2)}(\vec{x}, t) + \varepsilon^4 w^{(3)}(\vec{x}, t) \dots, \\ s(\vec{x}, t) &= \varepsilon^2 s^{(1)}(\vec{x}, t) + \varepsilon^3 s^{(2)}(\vec{x}, t) + \varepsilon^4 s^{(3)}(\vec{x}, t) \dots, \\ h(\vec{x}, t) &= \varepsilon^2 h^{(1)}(\vec{x}, t) + \varepsilon^3 h^{(2)}(\vec{x}, t) + \varepsilon^4 h^{(3)}(\vec{x}, t) \dots, \\ v_i(\vec{x}, t) &= \varepsilon v_i^{(1)}(\vec{x}, t) + \varepsilon^2 v_i^{(2)}(\vec{x}, t) + \varepsilon^3 v_i^{(3)}(\vec{x}, t) \dots \end{aligned} \tag{5}$$

Inserting Equation (5) into Equation (3) gives for the lowest-order functions

$$\begin{cases} \frac{\partial \Omega_i^{(1)}}{\partial t} = \Delta \Omega_i^{(1)}, \\ \frac{\partial w^{(1)}}{\partial t} = s^{(1)}, \\ \frac{\partial s^{(1)}}{\partial t} = \frac{1}{\gamma} \Delta w^{(1)} + \frac{4}{3} \Delta s^{(1)} - \frac{1}{\gamma} \Delta h^{(1)} + \psi_2^{(1)}, \\ \frac{\partial h^{(1)}}{\partial t} = \frac{\gamma}{Pr} \Delta h^{(1)} - (\gamma - 1) s^{(1)} + \psi_3^{(1)}. \end{cases} \tag{6}$$

$$\psi_2^{(1)} = \frac{\partial v_i^{(1)}}{\partial x_j} \frac{\partial v_j^{(1)}}{\partial x_i}, \psi_3^{(1)} = \frac{1}{2} \gamma (\gamma - 1) D_{ij} v^{(1)} D_{ij} v^{(1)}, D_{ij} v^{(1)} = \left(\frac{\partial v_i^{(1)}}{\partial x_j} + \frac{\partial v_j^{(1)}}{\partial x_i} \right).$$

The flow velocity is:

$$\begin{aligned} \vec{v}(\vec{x}, t) &= -\frac{0.25}{\pi} \int \left\{ \vec{\Omega}(\vec{x} + \vec{r}', t) \times \vec{n} + s(\vec{x} + \vec{r}', t) \vec{n} \right\} dr' \sin \theta' d\theta' d\varphi', \\ n &= \{ \sin \theta' \cos \varphi', \sin \theta' \sin \varphi', \cos \theta' \}. \end{aligned} \tag{7}$$

The System (6) consists of three homogeneous parabolic equations with respect to Ω_i (as a general rule) and a non-uniform parabolic subsystem with constant coefficients. One can find the solution to this subsystem using the Fourier transform.

The first equation of System (6) yields

$$\Omega_i^{(1)}(\vec{x}, t) = \frac{0.125}{\pi^{3/2}t^{3/2}} \int \Omega_i^{(1)}(\xi, 0) * exp\left(-0.25 \left|\vec{x} - \frac{\vec{\xi}}{t}\right|^2 / t\right) d\vec{\xi}. \tag{8}$$

In our case, only one component $\Omega_3^{(1)} = \Omega$ is different from zero.

Equation (8) allows us to determine the terms $\psi_2^{(1)}, \psi_3^{(1)}$ in Equation (6).

The Fourier transform of the homogeneous parabolic subsystem of (6) gives (the wavy line de-notes the Fourier transform):

$$\begin{cases} \frac{d\tilde{w}^{(1)}}{dt} = \tilde{s}^{(1)}, \\ \frac{d\tilde{s}^{(1)}}{dt} = -\frac{k^2}{\gamma}\tilde{w}^{(1)} - \frac{4}{3}k^2\tilde{s}^{(1)} + \frac{k^2}{\gamma}\tilde{h}^{(1)}, \\ \frac{d\tilde{h}^{(1)}}{dt} = -k^2\frac{\gamma}{Pr}\tilde{h}^{(1)} - (\gamma - 1)\tilde{s}^{(1)}. \end{cases} \tag{9}$$

The characteristic equation of the System (9) is [13]

$$f^3 + k^2\left(\frac{4}{3} + \frac{\gamma}{Pr}\right)f^2 + k^2\left(\frac{4}{3}\frac{\gamma}{Pr}k^2 + 1\right)f + \frac{k^4}{Pr} = 0 \tag{10}$$

The characteristic Equation (10) is a cubic one. It has one real root and two complex conjugate roots at $0 \leq k \leq k_*$.

At $0 \leq k \leq k_*, k_* \approx 1$ for air, the solutions of Equation (10) are

$$f_1 = \sigma_1(k), f_{2,3} = \sigma_2(k) \pm i\omega_r(k); \sigma_1, \sigma_2 < 0.$$

All the solutions are real and negative in the domain $k_* < k < \infty$.

They decay rapidly in a very short time, so we do not take this case into account. The dispersion curve $\omega_r(k)$ has two branches. We consider only the branch that corresponds to smaller values of the attenuation coefficients $\sigma_1, \sigma_2 (0 \leq k \leq k_1 < k_*)$.

The Fourier transform of the fundamental solution matrix for the parabolic Subsystem (9) is

$$\begin{aligned} A &= [a_{ij}], i = 1, 2, 3, \\ a_{1i} &= c_{1i}e^{\sigma_1 t} + c_{2i}e^{\sigma_2 t} \cos(\omega_r t) + c_{3i}e^{\sigma_2 t} \sin(\omega_r t), \\ a_{2i} &= c_{1i}\sigma_1 e^{\sigma_1 t} + (c_{2i}\sigma_2 + c_{3i}\omega_r)e^{\sigma_2 t} \cos(\omega_r t) + (c_{3i}\sigma_2 - c_{2i}\omega_r)e^{\sigma_2 t} \sin(\omega_r t), \\ a_{3i} &= c_{1i}\left(1 + \gamma\sigma_1\left(\frac{\sigma_1}{k^2} + \frac{4}{3}\right)\right)e^{\sigma_1 t} + \left(\left(1 + \frac{\gamma}{k^2}(\sigma_2^2 - \omega_r^2) + \frac{4}{3}\gamma\sigma_2\right)c_{2i} + \right. \\ &\quad \left. 2\gamma\omega_r\left(\frac{\sigma_2}{k^2} + \frac{2}{3}\right)c_{3i}\right)e^{\sigma_2 t} \cos(\omega_r t) + \left(-2\gamma\omega_r\left(\frac{\sigma_2}{k^2} + \frac{2}{3}\right)c_{2i} + \right. \\ &\quad \left. \left(1 + \frac{\gamma}{k^2}(\sigma_2^2 - \omega_r^2) + \frac{4}{3}\gamma\sigma_2\right)c_{3i}\right)e^{\sigma_2 t} \sin(\omega_r t). \end{aligned}$$

Here c_{ij} are defined from the initial conditions:

$$\begin{aligned} c_{11} &= (\gamma(\sigma_2^2 + \omega_r^2) - k^2)/g_1; c_{12} = -2(\sigma_2 + \frac{2k^2}{3})/g_0; c_{13} = \frac{k^2}{g_1}; \\ c_{21} &= (\gamma\sigma_1(\sigma_1 - 2\sigma_2) + k^2)/g_1; c_{22} = -c_{12}; c_{23} = -c_{13}; \\ c_{31} &= (\gamma\sigma_1(\sigma_2^2 - \sigma_1\sigma_2 - \omega_r^2) + k^2(\sigma_1 - \sigma_2))/(\omega_r g_1); \\ c_{32} &= (\sigma_1^2 - \sigma_2^2 + \omega_r^2 + 4k^2(\sigma_1 - \sigma_2)/3)/(\omega_r g_0); \\ c_{33} &= k^2(\sigma_2 - \sigma_1)/3)/(\omega_r g_1), g_0 = (\sigma_2 - \sigma_1)^2 + \omega_r^2, g_1 = \gamma g_0. \end{aligned}$$

In our case we investigate density oscillations. The function $w^{(1)}$ is

$$w^{(1)}(\vec{x}, t) = \frac{1}{2\pi\sqrt{\pi}} \int_0^t d\tau \int_{R^3} d\vec{\xi} \int_{R^3} d\vec{k} \exp\left(i\vec{k}(\vec{x} - \vec{\xi})\right) * \left\{ a_{12}(k, t - \tau)\psi_2^{(1)}(\vec{\xi}, \tau) + a_{13}(k, t - \tau)\psi_3^{(1)}(\vec{\xi}, \tau) \right\}, \tag{11}$$

The functions $\Omega_i^{(n)}, w^{(n)}(\vec{x}, t), s^{(n)}(\vec{x}, t), h^{(n)}(\vec{x}, t), n > 1$ can be obtained in the same manner.

Let us introduce the variable $\vec{X} = \vec{\xi} - \vec{x}_0$. With this new variable Equation (11) becomes

$$w^{(1)}(\vec{x}_0, t) = \sqrt{\frac{2}{\pi}} \int_0^t d\tau \int_0^{k_1} k dk \int_0^\infty R_3 dR_3 \int_0^\pi \sin\theta_3 d\theta_3 \int_0^{2\pi} d\varphi \sin(kR_3) * \left\{ a_{12}(k, t - \tau)\psi_2^{(1)}(\vec{x}_0 + \vec{X}, \tau) + a_{13}(k, t - \tau)\psi_3^{(1)}(\vec{x}_0 + \vec{X}, \tau) \right\}. \tag{12}$$

Density deviation from its initial value has the form $\frac{\rho_d - \rho_0}{\rho_0} = \frac{\rho_d}{\rho_0} - 1 \cong -w \cong -\omega_0^2 w^{(1)}$, here ρ_d denotes dimensional density.

Since $w \cong \omega_0^2 w^{(1)}$ and $w^{(1)}$ does not depend on the initial vorticity ω_0 , neither does the frequency of the acoustic radiation. The value ω_0 only affects the amplitude of w . The first terms of the series can be used for the analysis of frequency band of density oscillations in the case of low vorticity.

The coefficients of the power series by ω_0 are multiple integrals. The question of convergence of the series has not been investigated in this study.

3. Results

Equation (12) was used for the calculation of the density evolution. The multiple integrals were evaluated with the aid of Korobov grids [14].

The Korobov grids are elaborated for numerical evaluation of multiple integrals. Namely, integrals over a unit cube in R^n are considered.

The grids are as follows:

$$M_k = \left(\left\{ \frac{a_1 k}{p} \right\}, \dots, \left\{ \frac{a_s k}{p} \right\} \right), k = 1, 2, \dots, N.$$

where a_1, \dots, a_s are optimal coefficients.

The numbers $p = N$ and integer numbers a_1, \dots, a_s are mutually primes ones. The procedure of evaluating optimal coefficients is given in [14].

The discrepancy is proportional to $N^{-\alpha} \ln^\gamma N, \gamma = \gamma(\alpha, s), H_s^\alpha$ being the class of the functions under consideration.

The program code for calculating w and support functions was written in the Wolfram Language and was executed in Mathematica 5.0 program. The graphs and the spectra were built with the aid of the Qtiplot 0.9.9.2.

As shown, density oscillations arise. Computations refer to the initial domain inside the vortical cylinder as well as outside it. The process is different in these domains. There are high-frequency oscillations modulated by a low-frequency signal.

3.1. Low-Frequency Oscillations

Figures 1 and 2 demonstrate density oscillations inside the initial vortical cylinder.

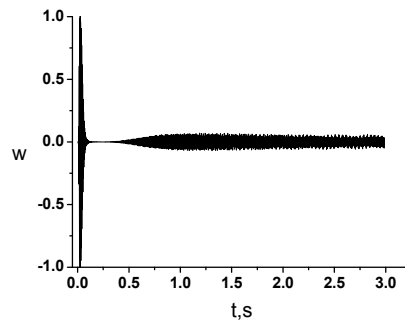


Figure 1. The oscillations inside the initial cylinder.

The value of $w = -\text{Log}\rho$ against time at the axis of the cylinder, $r_0 = 0.188$ cm, $z_0 = 2.909$ cm, $z = 1.7$ cm.

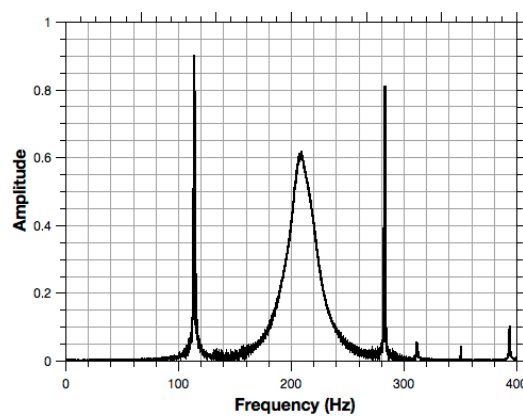


Figure 2. The oscillations inside the initial cylinder.

The oscillation spectrum of $w = -\text{Log}\rho$ at the cylinder axis ($r = 0$), $r_0 = 0.188$ cm, $z_0 = 2.909$ cm, $z = 1.7$ cm.

Figure 1 refers to the axis of the cylinder. As seen, the amplitude of the oscillations grows at first and then decays up to zero. Later on the oscillations arise anew. Figure 2 shows that there are two natural frequencies (about 115 Hz and 280 Hz) and a continuous spectrum.

Figure 3 represents the oscillations at the point $r = r_0/2$. As seen, there are two temporal intervals, in which the amplitude of the oscillations is large enough but the maximum amplitude is reached in the second area of oscillations. The oscillation spectrum (Figure 4) has two natural frequencies (about 115 Hz and 280 Hz), but there is no continuous spectrum.

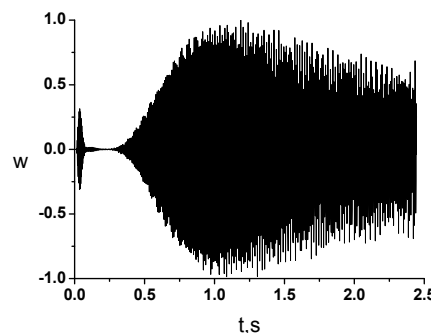


Figure 3. The oscillations inside the initial cylinder.

The value of $w = -\text{Log}\rho$ against time at $r = r_0/2$, $r_0 = 0.188$ cm, $z_0 = 2.909$ cm, $z = 1.7$ cm.

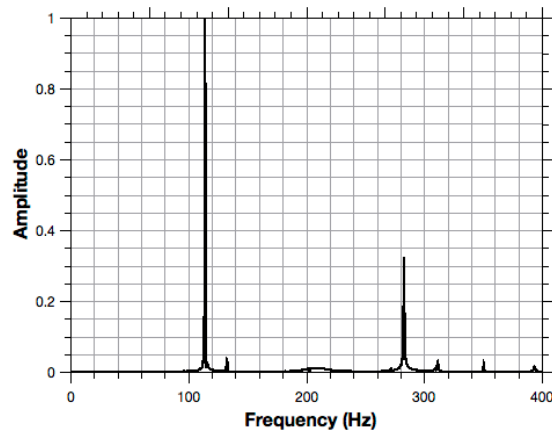


Figure 4. The oscillations inside the initial cylinder.

The oscillation spectrum of $w = -\text{Log}\rho$ at $r = r_0/2$, $r_0 = 0.188$ cm, $z_0 = 2.909$ cm, $z = 1.7$ cm.

The process is different in the flow outside the initial cylinder. Below we consider geometrically similar cylinders (Figures 5–8).

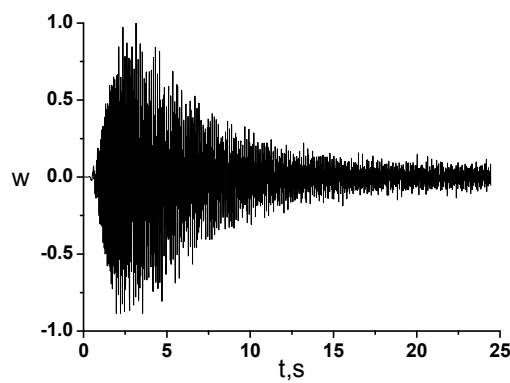


Figure 5. The scaling factor is equal to 1.

The value of $w = -\text{Log}\rho$ against time at $r > r_0$, $r = 1.709$ cm, $r_0 = 0.188$ cm, $z_0 = 2.909$ cm, $z = 1.7$ cm.

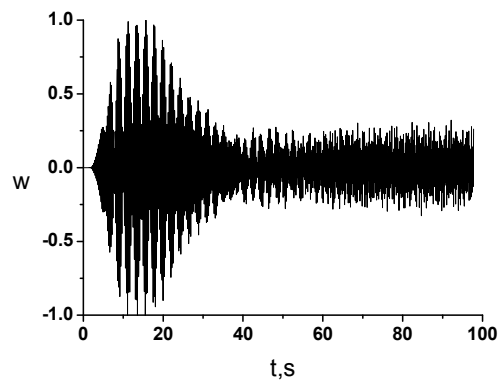


Figure 6. The scaling factor is equal to 2.

The value of $w = -\text{Log}\rho$ against time at $r > r_0$, $r = 3.418$ cm, $r_0 = 0.376$ cm, $z_0 = 5.818$ cm, $z = 3.4$ cm.

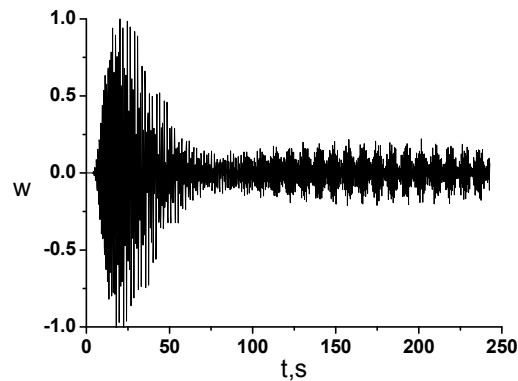


Figure 7. The scaling factor is equal to 3.

The value of $w = -\text{Log}\rho$ against time at $r > r_0$, $r = 5.127$ cm, $r_0 = 0.564$ cm, $z_0 = 8.727$ cm, $z = 5.1$ cm.

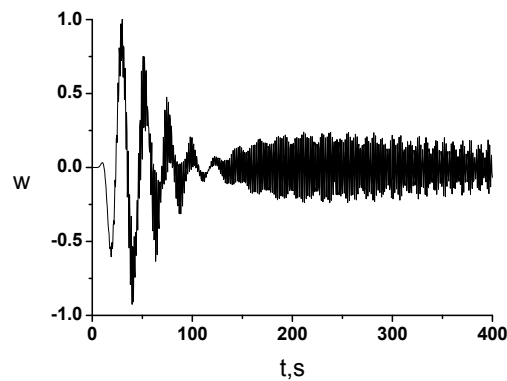


Figure 8. The scaling factor is equal to 4.

The value of $w = -\text{Log}\rho$ against time at $r > r_0$, $r = 6.836$ cm, $r_0 = 0.752$ cm, $z_0 = 11.636$ cm, $z = 6.8$ cm.

Figure 5 shows the oscillations at the point outside the cylinder. As can be seen, the oscillations grow at first (0–3 s), then a sharp decrease of amplitude takes place (3–12 s). Further on saturation occurs and then the oscillations decay slowly. The radiation starts when the wave arrives at the observation point.

Let us consider the acoustic radiation from cylinders with scaling factors 2, 3 and 4.

The process in Figure 6 (the scaling factor is 2) is almost identical to the original one, but it develops slowly. The increase of the amplitude occurs in the interval 0–15 s. Later on, the amplitude decreases.

If the scaling factor is equal to 3 (Figure 7), the process occurs more slowly than the previous one. In addition, one can observe two areas of increase of the oscillation amplitude: namely, 0–25 s and 80–160 s.

Figure 8 corresponds to a scaling factor 5. Clearly, the area of the determination of oscillations (0–110 s) is shown. Then, as in the previous cases, there is a region of steady oscillations with gradually decreasing amplitude.

The acoustic oscillations are pressure fluctuations. In our case the density dependence is similar to that of the pressure. The intensity of acoustic radiation is proportional to the square of density fluctuations.

The spectrum of the oscillations represented in Figure 5 is given in Figure 9. There are two natural frequencies (17 Hz and 24 Hz).

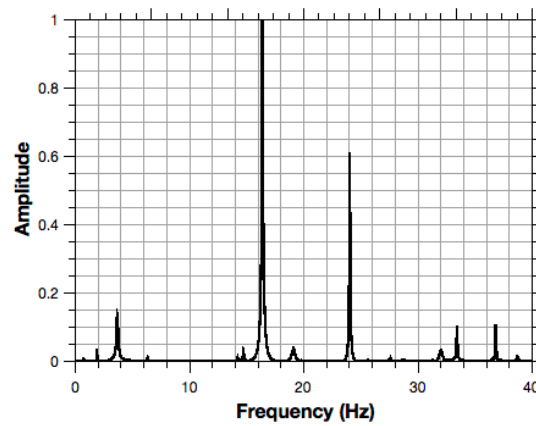


Figure 9. The oscillations outside the initial cylinder.

The oscillation spectrum of $w = -\text{Log}\rho$ at $r > r_0$, $r = 1.709$ cm, $r_0 = 0.188$ cm, $z_0 = 2.909$ cm, $z = 1.7$ cm.

3.2. High-Frequency Oscillations

Furthermore, one can observe high-frequency oscillations (Figures 10 and 11). Once again, two high characteristic frequencies are observed for different vortex radii: 920 and 1120 Hz ($r_0 = 0.188$ cm, Figure 12), 790 Hz and 1150 Hz ($r_0 = 2$ cm, Figure 13).

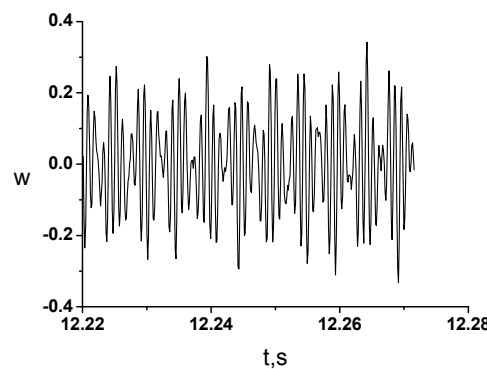


Figure 10. High-frequency oscillations. The scaling factor is equal to 1.

The value of $w = -\text{Log}\rho$ against time at $r > r_0$, $r = 1.709$ cm, $r_0 = 0.188$ cm, $z_0 = 2.909$ cm, $z = 1.7$ cm.

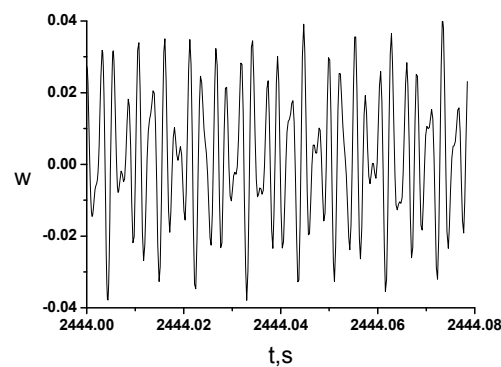


Figure 11. High-frequency oscillations. The scaling factor is equal to 10.6.

The value of $w = -\text{Log}\rho$ against time at $r > r_0$, $r = 18.12$ cm, $r_0 = 2$ cm, $z_0 = 30.84$ cm, $z = 18.02$ cm.

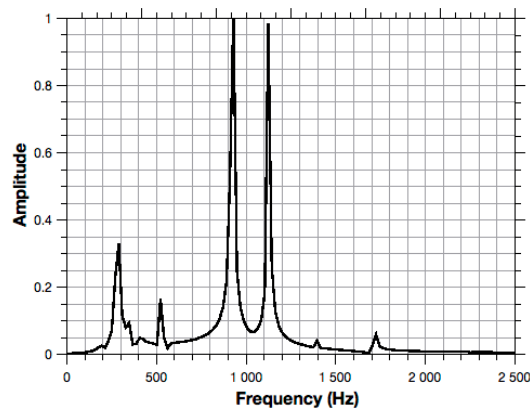


Figure 12. High-frequency oscillations. The scaling factor is equal to 1.

The oscillation spectrum of $w = -\text{Log} \rho$ at $r > r_0$, $r = 1.709$ cm, $r_0 = 0.188$ cm, $z_0 = 2.909$ cm, $z = 1.7$ cm.

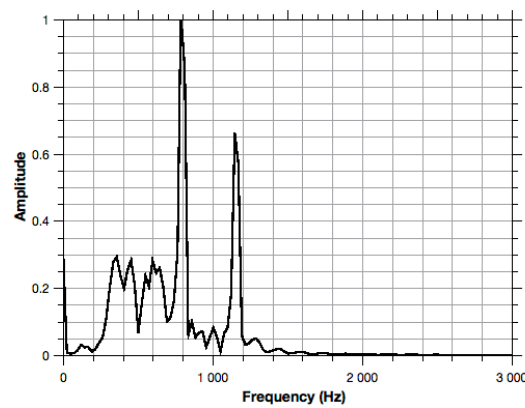


Figure 13. High-frequency oscillations. The scaling factor is equal to 10.6.

The oscillation spectrum of $w = -\text{Log} \rho$ at $r > r_0$, $r = 18.12$ cm, $r_0 = 2$ cm, $z_0 = 30.84$ cm, $z = 18.02$ cm.

It is important to note that the high-frequency oscillations as well as the low-frequency ones have two natural frequencies. The occurrence of two-period oscillations can be explained by two characteristic sizes (radius and height) of the cylinder.

4. Discussion

The dependence of low-frequency oscillations of scaling factor is presented in Figure 14. It shows that the frequency decreases exponentially with increasing scaling factor.

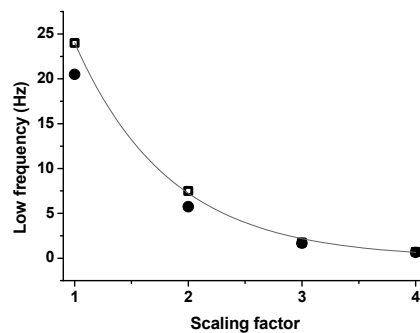


Figure 14. High-frequency oscillations. Dependence of the oscillation frequency on the scaling factor.

Unfortunately, there are no available experimental data referring to acoustic radiation of vertical gaseous cylindrical vortices.

Therefore, we compared our results with experimentally observed frequencies of vortex rings and frequency of turbulent atmospheric fluctuations.

The atmospheric frequencies are in the 0.5–290 Hz range [15]. According to our data, the low-frequency oscillations of the vortex cylinder are in the 17–280 Hz range.

The high-frequency oscillations were already theoretically observed in another paper [16]. We compared the high-frequency oscillations with the acoustic radiation of turbulent vortex rings [17].

The vortex rings investigated in the other paper [17] were generated in an anechoic chamber by means of a piston-driven vortex generator with a nozzle diameter $d = 4$ cm and an initial jet ejection velocity 30 ms^{-1} (corresponding to Reynolds number $Re = 6.8 \times 10^4$). The ring noise was determined from the averaged spectrum in a series of 12 selected time samples of length 31.2 ms starting after 220 ms from the initiation of the ring (this corresponds to the part of the path at a distance from 200 to 230 cm from the nozzle orifice), manifesting itself as strong peaking of the spectrum in a narrow frequency band ($\Delta\omega = 300$ Hz) with the maximum near the frequency $\omega_0 = 1200$ Hz.

This value coincides with our results for cylinder radius 2 cm (Figures 11 and 13) (high-frequency oscillations for vortex cylinder are 790 and 1150 Hz).

It also is interesting to note that the acoustic radiation of jets refers to the Strouhal number ($St = fL/v$; here, L and v are the characteristic size and the characteristic speed, respectively, f is frequency) in the range $St = 0.1$ – 0.2 [18]. It corresponds well to the Strouhal number in our calculations, which is in the 0.01–0.7 range.

5. Conclusions

On the basis of the Navier–Stokes equations, for the first time, the problem of the acoustic radiation of a single vortical cylinder in viscous heat-conducting gas has been solved. The solution has been obtained in the form of a power series in the initial vorticity ω_0 , multiple integrals being the appropriate coefficients. The first-order term of the series represents the solution, if $\omega_d \ll c_0^2/d$, where the subscript “ d ” denotes the dimensional value and c_0 is the low-frequency sound speed referred to the initial state.

The validation of the results has been provided using modern methods. The Korobov grid has been used for calculations. The accuracy of the Korobov method is higher than that of Monte–Carlo.

The analysis of the acoustic radiation of a single vortical cylinder has led to the following conclusions:

- (i) It was found that there are high and low frequencies corresponding to the frequencies experimentally observed for the vortex ring and atmospheric frequencies, respectively.
- (ii) As seen, the pattern of oscillations is different inside the initial cylinder and outside it. This fact may be explained as follows. There are multiple reflections of acoustic waves inside the initial cylinder. The reflected waves must be weaker in the domain outside.
- (iii) There are high-frequency oscillations modulated by a low-frequency signal. The value of high frequency remains constant during a long time. Thus it is possible to consider the high frequency as the natural frequency of the vortex. The value of the natural frequency depends on the initial radius of the vortical cylinder and does not depend on the intensity of the initial vorticity. Namely, it diminishes if the radius of the cylinder increases, as expected from physical considerations. The natural frequency has different values inside the initial cylinder and in the outer domain.

Hitherto, researchers analyzed sound generation under vortex–vortex and vortex–acoustic generation interactions. We considered sound generation by a single vortex due to vortex diffusion. The results of the paper may be of interest for aeroacoustics and tornado modeling.

Acknowledgments: Comments by Olga Azarova and Natalia Suhareva are gratefully acknowledged.

Author Contributions: Both of the authors contributed equally to this paper.

Conflicts of Interest: The authors declare no conflict of interest.

References

1. Lighthill, M.J. On Sound Generated Aerodynamically. I. General theory. *Proc. Roy. Soc.* **1952**, *211*, 564–587. [[CrossRef](#)]
2. Powell, A. Vortex Sound Theory. *J. Acoust. Soc.* **1964**, *36*, 177–195. [[CrossRef](#)]
3. Inoue, O. Sound Generation by the Leapfrogging between Two Coaxial Vortex Rings. *Phys. Fluids* **2002**, *14*, 3361–3364. [[CrossRef](#)]
4. Eldredge, J.D. The Dynamics and Acoustics of Viscous Two-Dimensional Leapfrogging Vortices. *J. Sound Vibrat.* **2007**, *301*, 74–92. [[CrossRef](#)]
5. Eldredge, J.D.; Colonius, T.; Leonard, A. A Vortex Particle Method for Two-Dimensional Compressible Flow. *J. Comput. Phys.* **2002**, *179*, 371–399. [[CrossRef](#)]
6. Arnold, V.I. Conditions for Non-Linear Stability of Plane Stationary Curvilinear Flows of an Ideal Fluid. *Dokl. Akad. Nauk SSSR.* **1965**, *162*, 773–777. (In Russian)
7. Johnson, G.M. An Empirical Model of the Motion of Turbulent Vortex Rings. *AIAA J.* **1971**, *9*, 763–764. [[CrossRef](#)]
8. Maxworthy, T.J. Turbulent Vortex Rings. *J. Fluid Mech.* **1974**, *64*, 227–240. [[CrossRef](#)]
9. Maxworthy, T.J. Some Experimental Studies of Vortex Rings. *J. Fluid Mech.* **1977**, *81*, 465–495. [[CrossRef](#)]
10. Dearnorff, J.W. A Numerical Study of Three-Dimensional Turbulent Channel Flow at Large Reynolds Numbers. *J. Fluid Mech.* **1970**, *41*, 453–480. [[CrossRef](#)]
11. Thomson, W. XXIV. Vibration of a Columnar Vortex. *J. Phil. Mag.* **1880**, *10*, 155–168. [[CrossRef](#)]
12. Yakovlev, P.G. Sound Radiation by a Plane Localized Vortex. *Acoust. Phys.* **2012**, *58*, 516–520. [[CrossRef](#)]
13. Truesdell, C. Precise Theory of the Absorption and Dispersion of Forced Plane Infinitesimal Waves According to the Navier–Stokes Equations. *J. Ration. Mech. Anal.* **1953**, *2*, 643–741. [[CrossRef](#)]
14. Korobov, N.M. *Theoretical and Numerical Methods in Approximate Analysis*; Moscow Center of Mathematical Education: Moscow, Russia, 2004. (In Russian)
15. Tatarskii, V.I. *Wave Propagation in the Turbulent Medium*; McGraw–Hill: New York, NY, USA, 1961.
16. Petrova, T.A.; Shugaev, F.V. Acoustic Radiation Frequency of a Cylindrical Vortex. *Mosc. Univ. Phys. Bull.* **2015**, *70*, 245–250. [[CrossRef](#)]
17. Kopiev, V.F.; Chernyshev, S.A. Vortex Ring Eigen-Oscillations as a Source of Sound. *J. Fluid Mech.* **1997**, *341*, 19–57. [[CrossRef](#)]
18. Lebedev, M.G.; Telenin, G.F. *Frequency Characteristics of Supersonic Jets*; Moscow University Press: Moscow, Russia, 1978. (In Russian)



© 2016 by the authors; licensee MDPI, Basel, Switzerland. This article is an open access article distributed under the terms and conditions of the Creative Commons Attribution (CC-BY) license (<http://creativecommons.org/licenses/by/4.0/>).